Competition between the inter- and intra-sublattice interactions in Yb_{2}V_{2}O_{7}

Z. L. Dun, J. Ma, H. B. Cao, Y. Qiu, J. R. D. Copley, T. Hong, M. Matsuda, J. G. Cheng, M. Lee, E. S. Choi, S. Johnston, and H. D. Zhou

Phys. Rev. B **91**, 064425 — Published 27 February 2015

DOI: 10.1103/PhysRevB.91.064425

Competition between the inter- and intra-sublattice interactions in $Yb_2V_2O_7$

Z. L. Dun,[1] J. Ma,[2] H. B. Cao,[2] Y. Qiu,[3,4] J. R. D. Copley,[3] T. Hong,[2] M. Matsuda,[2]
J. G. Cheng,[5] M. Lee,[6,7] E. S. Choi,[7] S. Johnston,[1,8] and H. D. Zhou[1,7]

[1]*Department of Physics and Astronomy, University of Tennessee, Knoxville, Tennessee 37996-1200, USA*
[2]*Quantum Condensed Matter Division, Oak Ridge National Laboratory, Oak Ridge, Tennessee 37381, USA*
[3]*NIST Center for Neutron Research, Gaithersburg, Maryland, 20899-6102, USA*
[4]*Department of Materials Science and Engineering, University of Maryland, College Park, Maryland, 20742, USA*
[5]*Beijing National Laboratory for Condensed Matter Physics, and Institute of Physics, Chinese Academy of Sciences, Beijing 100190, China*
[6]*Department of Physics, Florida State University, Tallahassee, FL 32306-3016, USA*
[7]*National High Magnetic Field Laboratory, Florida State University, Tallahassee, FL 32310-3706, USA*
[8]*Joint Institute for Advanced Materials, The University of Tennessee, Knoxville, 425 Dougherty Engineering Building, Knoxville, TN 37996, USA*

(Dated: February 5, 2015)

We studied the magnetic properties of single crystal $Yb_2V_2O_7$ using dc and ac susceptibility measurements, elastic and inelastic neutron scattering measurements, and linear spin wave theory. The experimental data shows a ferromagnetic ordering of V^{4+} ions at 70 K, a short-range ordering of Yb^{3+} ions below 40 K, and finally a long-range non-collinear ordering of Yb^{3+} ions below 15 K. With external magnetic field oriented along the [111] axis, the Yb-sublattice experiences a spin flop transition related to the "three-in one-out" spin structure. By modeling the spin wave excitations, we extract the Hamiltonian parameters. Our results confirm that although the extra inter-sublattice Yb-V interactions dramatically increases the Yb ordering temperature to 15 K, the intra-sublattice Yb-Yb interactions, based on the pyrochlore lattice, still stabilize the Yb ions' non-collinear spin structure and spin flop transition.

PACS numbers: 75.25.-j, 75.40.Gb, 75.40.-s, 78.70.Nx

I. INTRODUCTION

The search for quantum spin liquid (QSL) states in real materials is a major goal of modern condensed matter physics[1]. For a long time efforts have focused on two-dimensional triangular[2–5] and kagome[6–8] lattices hosting low-spin magnetic ions, however, recently the search has been extended to the quantum spin ice on the pyrochlores with strong quantum fluctuations. In this context, the three-dimensional pyrochlore $Yb_2Ti_2O_7$ has received a lot of attention as a possible QSL candidate[9–21]. A number of attempts have been made to extract the spin Hamiltonian of the Yb spins from experiments[9,10,13–15]. Recent work extracted model parameters by fitting the spin waves excitations of $Yb_2Ti_2O_7$ in a magnetic field as measured by inelastic neutron scattering[14] and this model has been further validated in a number of subsequent works[10,15]. In this case, the exchange interactions between the effective spin-$\frac{1}{2}$ Yb^{3+} are of the frustrated ferromagnetic type and a non-collinear ferromagnetic ground state is predicted. In the real material, however, the situation is more complicated. A low-temperature phase transition ($T \sim 250$ mK) has been observed[11–13,16,21], but the nature of this state — a true QSL or a partially understood ferromagnetic phase-is unclear at this time. But one thing is generally agreed upon: the ground state is fragile and easily perturbed by site disorder, applied magnetic field, chemical pressure, and so forth. It is therefore important to study various perturbations of the Yb sublattice.

We grew studied crystals of $Yb_2V_2O_7$ in order to examine the influence of the magnetically active V^{4+} ion on the Yb pyrochlore sublattice. Previous studies of the $R_2V_2O_7$ (R = Ho, Er, Yb, Lu, and Y) series have demonstrated that the V^{4+} ions order ferromagnetically at $T \sim 70$ K with a fully saturated moment ($1\mu_B$ for V^{4+} ion)[22–25]. A similar high-T ordering is observed here. We also expect an additional inter-sublattice Yb-V interaction that will affect the ground state of Yb^{3+} ions at low temperatures. Indeed, prior polycrystalline $Yb_2V_2O_7$ studies indicate that there is a ferromagnetic ordering of Yb^{3+} ions around 30 K[24,25] in addition to the V^{4+} ordering at ~ 70 K. This indicates that the Yb-V interactions can dramatically affect the Yb ions in comparison to the enigmatic state found in $Yb_2Ti_2O_7$. Several important questions remain, however. For example, what are the ordering processes and what is the spin structure of Yb^{3+} ions? How do the additional inter-sublattice interactions modify the Hamiltonian of the Yb sublattice? And, more importantly, do the Yb-Yb interactions compete with the Yb-V interactions and if so, what signatures does this leave on the ground state? We address these questions here through a combination of detailed measurements of the magnetic properties of single crystalline $Yb_2V_2O_7$ and theory.

II. EXPERIMENTS SETUP

The single crystal sample of $Yb_2V_2O_7$ was grown using optical floating-zone method in a purified Argon atmosphere. Starting material Yb_2O_3, V_2O_3 and V_2O_5 powder was first mixed at proper ratio and then pre-reacted in an evacuated quartz tube at 1200°C for 40h before the growth in image furnace. A best growth was achieved with a pulling speed of 15mm/h. The crystals were oriented by Laue back diffraction.

The dc magnetic-susceptibility was measured with a Quantum Design[26] dc SQUID magnetometer with μ_0H = 0.05 T. The ac susceptibility and magnetization measurements down to 20 mK were performed on a home-made set up at SCM1 of National High Magnetic Field Laboratory.

Single crystal neutron diffraction was measured at the Four-Circle Diffractometer(HB-3A)[27] of High Flux Isotope Reactor(HFIR), Oak Ridge National Laboratory(ORNL). Neutron wavelength of λ = 1.003 Å was used with a bent perfect Si-331 monochromator. The data was collected at 100 K, 40 K, 4 K and refined though program Fullprof-suit. The linear ferromagnetic structure of V^{4+} was confirmed by 40 K data and the ground state moment of Yb^{3+} was refined from 4 K data. The temperature dependence of Bragg Peak intensity was measured by fixing the detector at each Bragg peak center with a temperature rising scan.

Inelastic single crystal neutron scattering experiments were completed at Fixed-Incident-Energy Triple-Axis Spectrometer(HB1-a), the cold neutron triple-axis spectrometer (CTAX) of HFIR, ORNL and the NIST center for neutron scattering using the Disk Chopper Spectrometer (DCS)[28] and Multi-axis crystal spectrometer (MACS)[29]. The MACS experiment with a higher neutron flux gives a better resolution of spin waves, as shown in Figs. 5. In the MACS experiment setup, a 2 g single crystal $Yb_2V_2O_7$ was aligned in HHL plane. The spin wave dispersion was mapped out by measuring the Q-dependent scattering in HHL plane with different energy transfer ΔE. We used a fixed final energy E_f = 2.35 meV and varied the incident energy E_i from 2.35 meV to 5.05 meV with 0.15 meV per step, which made ΔE range from 0 to 2.7 meV. The instrument energy resolution was 0.0787 meV and Q resolution 0.086Å^{-1}(energy resolution corresponds to the elastic energy resolution, and the Q resolution corresponds to the value at **Q**=(111) in reciprocal lattice space). Data was collected at 1.5 K and 40 K. The spin wave spectrum was obtained by subtracting the 1.5 K data by 40 K data, eliminating the elastic scattering and detector background.

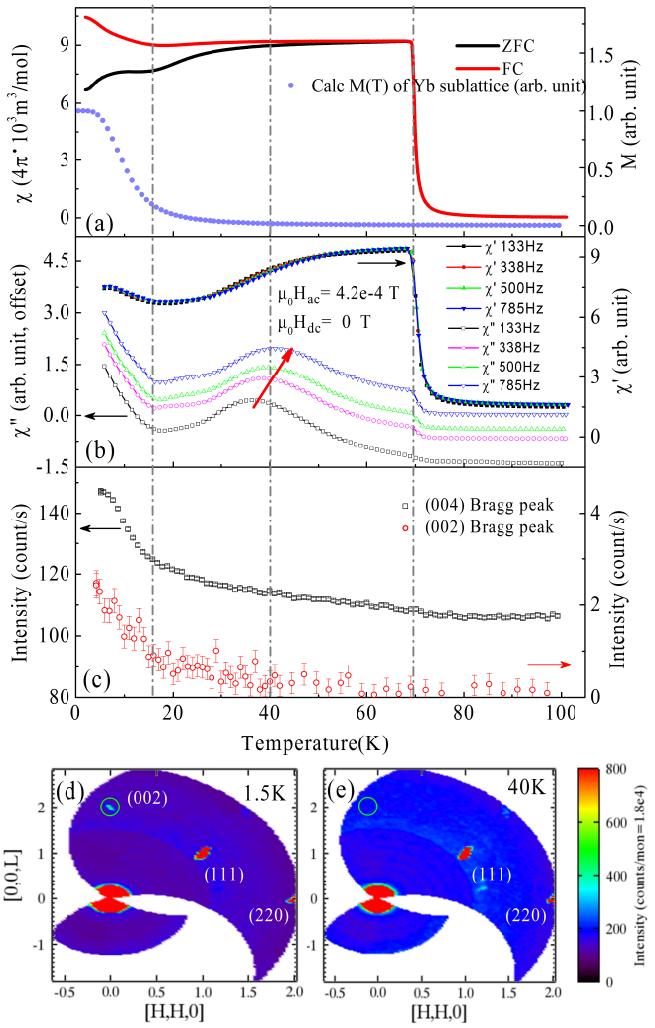

FIG. 1: (color online) (a) Temperature dependence of the dc susceptibility $\chi(T)$ measured with μ_0H = 0.05 T. Blue circles: Calculated temperature dependence of magnetization M(T) of Yb sublattice. (b) Temperature dependence of the real χ' and imaginary χ'' parts of the ac susceptibility measured under $\mu_0 H_{ac}$ = 4.2e-4 T with different frequencies. The χ'' data is offset by each other; (c) Temperature dependence of the (002) and (004) Bragg peaks' intensity obtained from single crystal neutron diffraction experiments. Three ordering temperatures (70 K, 40 K, and 15 K) are marked as dashed lines. (d)The elastic channel(-0.1meV $\leq \Delta E \leq$ 0.1 meV) of the neutron scattering data collected at MACS for T = 1.5 K and (e)T = 40 K, the (002) Bragg peak position is highlighted with green circle. Error bars in the figure represent one standard deviation.

III. ORDERING PROCESS OF V^{4+} AND YB^{3+} SUBLATTICE

The dc magnetic susceptibility $\chi(T)$ of $Yb_2V_2O_7$ (Fig. 1a) shows a sharp transition at 70 K, followed by a field cooling (FC) and zero field cooling (ZFC) divergence below 40 K, and another anomaly below 15 K. The ac susceptibility χ' correspondingly shows a sharp transition at 70 K and an increase below 15 K. The imaginary part χ'' shows another additional broad peak around 40 K. With increasing frequency, this peak around 40 K shifts

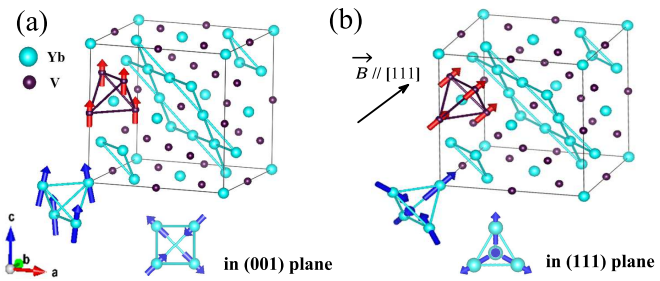

FIG. 2: (color online) The spin configuration of the Yb^{3+} and V^{4+} sublattices in (a) zero field and (b) with an applied magnetic field along [111] axis after the spin flop transition.

to higher temperatures while the increase at 15 K does not. It has been established that the 70 K transition in the $R_2V_2O_7$ series is a fully developed collinear ferromagnetic ordering of the V^{4+} ions[22,24,25,30,31]. The 40 K and 15 K features are therefore related to the development of the magnetic correlations of the Yb^{3+} ions. The FC and ZFC divergence of χ, plus the frequency dependent ac susceptibility peak of χ'', shows that the 40 K feature is a cluster behavior-like short-range ordering of Yb^{3+} ions. The frequency independence of the increase at 15 K indicates that this feature is a long-range ordering of the Yb sublattice.

The hierarchy of orderings are further confirmed by elastic single crystal neutron diffraction. In $Yb_2V_2O_7$, the (004) peak represents a lattice Bragg peak while the (002) peak is forbidden in the $Fd\bar{3}m$ space group. Below 70 K, the (004) peak intensity begins to increase due to the ferromagnetic ordering of V^{4+} ions, while the (002) peak intensity stays below the noise floor (Fig. 1c). Below 40 K, the intensity of (002) peak begins to increase, in addition to the continued increase of the intensity of (004) peak. These behaviors signal a short range ordering of the Yb^{3+} ions, consistent with previous neutron powder diffraction studies that reported a ferromagnetic ordering of Yb^{3+} ions around 30 K[24]. At 15 K, the intensity of the (002) and (004) peaks experiences a rapid increase, which is strong evidence of Yb^{3+} long-range ordering. The (002) magnetic Bragg peak is also clearly observed in the elastic channel of the neutron scattering pattern. A weak (002) Bragg peak presents at $T = 1.5$ K and absent at $T = 40$ K (Fig. 1(d, e)). The presence of a (002) Bragg peak confirms that the Yb^{3+} spins do not have a simple collinear ferromagnetic structure, but instead have additional canted antiferromagnetic components below 15 K.

Our refinement results based on the 40 K and 2 K magnetic Bragg peaks further support the notion that the 15 K increase in the magnetization is due to an ordering of the Yb sublattice, yielding the zero-field spin configuration shown in Fig 2a. The V^{4+} spins have a simple collinear ferromagnetic structure along one major axis ([001]). The Yb^{3+} spins have a major ferromagnetic component along the same direction, however, they tilt away from [001] axis forming a non-collinear ferromagnetic spin structure. Here, the Yb^{3+} spins form an antiferromagnetic "two-in-two-out" configuration within each tetrahedron in the plane perpendicular to the direction of the V^{4+} moment. This accounts for the (002) Bragg peak. The resolved moment for each Yb^{3+} ion is $\vec{M}$=(±0.16,±0.16,0.94)μ_B in the global coordinate frame.

IV. MAGNETIZATION AND SPIN FLOP TRANSITION

Magnetization curves of $Yb_2V_2O_7$ measured with the applied field along three different directions are shown in Figs. 3. At T= 60 K, the 0.6 μ_B moment of V^{4+} is quickly reached in all directions around a small field of 0.06 T, indicating a weak anisotropy of V^{4+} sublattice. The Yb^{3+} paramagnetism then follows, adding a linear contribution of the magnetization curve. At $T = 0.6$ K, the moment of each (V+Yb) approaches $M_{c3} = 2.7$ μ_B at 5 T. Previous study on $Lu_2V_2O_7$[31] has shown that its magnetization measured at 5 K saturates around 0.1 T with a value of 1.0 μ_B/V^{4+}. This indicates that 1.0 μ_B of the low temperature saturation moment comes from the V^{4+} and 1.7 μ_B is contributed by Yb^{3+} in $Yb_2V_2O_7$. The 1.7μ_B Yb^{3+} saturation moment is consistent with that of $Yb_2Ti_2O_7$, showing that $Yb_2V_2O_7$ has the similar crystal fields as $Yb_2Ti_2O_7$, in which the ground state is formed from a well isolated Kramers doublet with the effective spin-$\frac{1}{2}$ Yb^{3+} ions[17,18,24].

Fig. 4(a, b) show the enlarged dc magnetization and related derivatives at 0.6 K for applied fields along the [100], [110], and [111] axis. The magnetization along [111] shows a slope change around $\mu_0H_{c1} = 0.15$ T, which is also evidenced as a kink in its derivative curve. The ac magnetization measured at 20 mK with field along [111] shows two distinct kinks around 0.15 T and $\mu_0H_{c2} = 0.4$ T, which are absent from the [100] and [110] directions. The field dependence of the magnetic torque measured with H ∥ [111] also reveals a superlinear rise around H_{c1} with a peak on its derivative. The corresponding magnetization of these two critical fields in Fig. 4a are M_{c1} = 1.6μ_B/(Yb+V) at μ_0H_{c1} and M_{c2} = 2.2μ_B/(Yb+V) at μ_0H_{c2} . Subtracting 1μ_B from the V^{4+} ion, the Yb^{3+} moment is then $M_{c1,Yb} = 0.6\mu_B$ and $M_{c2,Yb} = 1.2\mu_B$. $M_{c1,Yb}$ is the average value of four Yb^{3+} moment along [111] direction in a tetrahedron, $M_{c2,Yb}$ is consistent with the free moment of Yb^{3+} ($\sim$ 1.15 μ_B)[17]. H_{c1} therefore represents a spin flop transition to half of the full Yb^{3+} moment and H_{c2} represents the entrance to the full polarization phase.

The spin flop process is illustrated in Fig. 2b. Due to the easy anisotropy of V^{4+} sublattice, all the V^{4+} spins flip to [111] direction under a small magnetic field applied along [111] (magnetization recovers 1 μ_B at 0.06 T). As the field increases, the Yb^{3+} moments enter a "three-in-one-out" or "three-out-one-in" spin configuration around

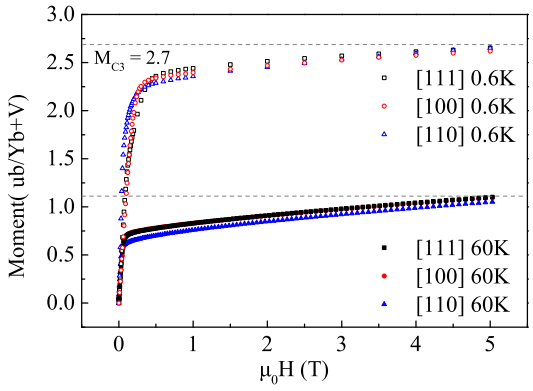

FIG. 3: (Color Online) The dc magnetization of $Yb_2V_2O_7$ measured at 60 K and 0.6 K with external magnetic field applied along three different axis [111], [110] and [100]. M_{c3} represents the saturation moment measured at 0.6 K.

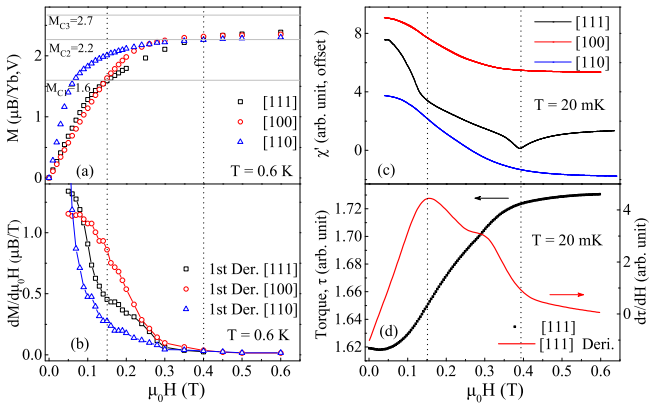

FIG. 4: (color online) Field dependence of (a) the dc magnetization M measured at 0.6 K and (b) its derivative. (c) Field dependence of the real part of ac susceptibility ($\mu_0 H_{ac}$ = 4.2e-4 T) measured at 20 mK. The data is offset by each other; (d) Field dependence of the magnetic torque measured with H ∥ [111] and its derivative. The external field H is applied along the [111], [110], and [100] axis. Two critical fields 0.15 T, 0.4 T are indicated by the dashed lines, and M_{c1}, M_{c2} represent the moments at corresponding fields. M_{c3} represents the moment measured at 5 T in Fig. 3.

H_{c1}. For this Yb^{3+} spin configuration, the effective spin within a tetrahedron along [111] is half the value of the full spin moment. In fact, the observed dc and ac magnetization are very similar to those of the spin ice pyrochlore $Dy_2Ti_2O_7$ measured at 1.8 K, which is the first example showing this "three-in-one-out" state[32]. One comment is that in $Dy_2Ti_2O_7$, with cooling temperature down to 0.35 K, the "three-in-one-out" state leads to a magnetization plateau for a field H ≤ 1 T[33]. We have not observed clear features of the magnetization plateau at 0.6 K for $Yb_2V_2O_7$. This indicates that the spin flop transition in $Yb_2V_2O_7$ survives within a narrow field regime.

V. SPIN WAVE EXCITATION

Next we examined the spin wave excitations in $Yb_2V_2O_7$ using inelastic neutron scattering (INS) experiments and linear spin wave theory. The spin-excitation spectra at 1.5 K along several high-symmetry directions within the HHL scattering plane are shown in Fig. 5. Here, the magnetic scattering intensities contributed from the Yb^{3+} ions was obtained by subtracting data taken at 40 K as background. We observe well defined spin wave excitations dispersing in energy between 1 and 2.2 meV.

We modeled these excitations using spin wave theory similar to Ref. 14 and complete details are given in the appendix. The Hamiltonian is assumed to have the form

$$H = H_{\mathrm{V-V}} + H_{\mathrm{Yb-Yb}} + H_{\mathrm{V-Yb}}. \qquad (1)$$

The three terms describe the intra-sublattice interactions on the V and Yb sublattices, and the inter-sublattice interactions, respectively. Since we are primarily interested in the low-T dynamics of the Yb sublattice, we freeze the V spins into their ferromagnetic arrangement and neglect $H_{\mathrm{V-V}}$ for $T \ll 70$ K. We assume that $H_{\mathrm{Yb-Yb}}$ is given by nearest-neighbor exchange couplings only[14] and that the effective Yb spins couple to a mean-field V spin $\langle S_{\mathrm{V}} \rangle$ via a ferromagnetic exchange coupling $J_{\mathrm{Yb-V}}$[24,43]. The resulting effective low-T Hamiltonian is

$$H = \frac{1}{2}\sum_{ij} J_{ij}^{\mu\nu} S_i^{\mu} S_j^{\nu} + \sum_i J_{Yb-V} S_i^z \langle S_V \rangle, \qquad (2)$$

where we have used global spin coordinates and set $\hbar = 1$. The intra-Yb sublattice interactions are specified by four independent exchange constants J_α, $\alpha = 1, \cdots, 4$ (See Appendix).

We obtain the spin wave dispersion from Eq. (2) using linear spin wave theory as outlined in Ref. 14. The primary difference is that here $\langle S_V \rangle$ plays the role of the applied magnetic field although it has a similar effect in stabilizing the Yb magnetic order. The classical ground state of the Yb sublattice is found by minimizing Eq. (2) with respect to the spin orientation. Guided by our experimental refinement of the magnetic Bragg peaks, we assumed that the ground state does not enlarge the unit cell. The spin-wave excitations are then calculated by expanding about this solution with Holstein-Primakoff transformation, which is truncated to order $s = 1/2$. The values of the exchange constants J_α and J_{Yb-V} are found by fitting the resulting spin-wave dispersions to the INS data. We obtain (in meV) $J_1 = -0.201$, $J_2 = -0.534$, $J_3 = -0.507$, $J_4 = 0.09$, and $J_{\mathrm{Yb-V}} = 0.76$. These correspond to values of (in meV) $J_{zz} = 0.173$, $J_{\pm} = 0.076$, $J_{\pm\pm} = 0.076$, and $J_{z\pm}$ = -0.314 for the intra-Yb lattice interactions in the local spin coordinates[14]. The calculations (top row, Fig. 5) reproduce many features of the

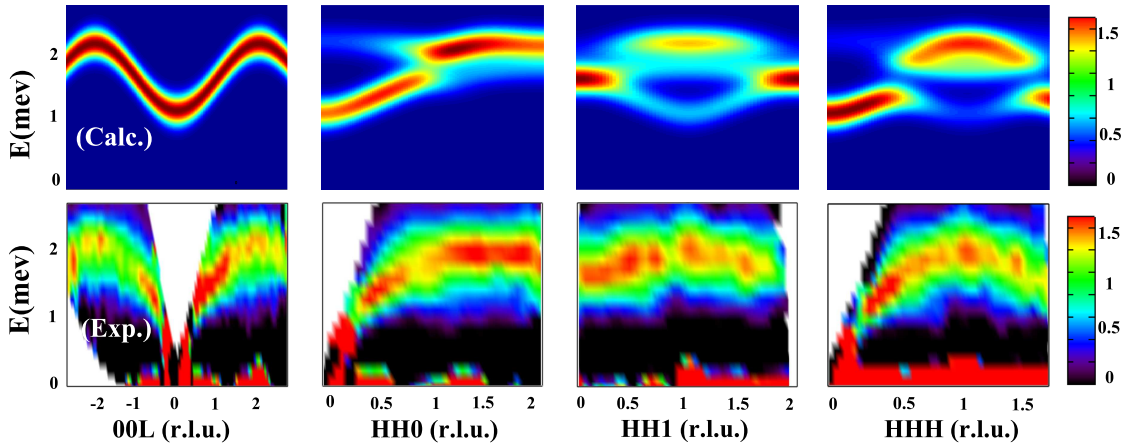

FIG. 5: (color online) Lower panels: the measured inelastic neutron scattering S($\mathbf{Q}$,ω) at 1.5 K, sliced along various directions in the HHL plane. Upper panels: the corresponding calculated S($\mathbf{Q}$,ω) convoluted with a Gaussian of full-width 0.15 meV(chosen to meet the spin wave width observed) adopting the exchange parameters in the main text. (r.l.u stands for reciprocal lattice unit.)

measured spin wave excitations (bottom row) including their overall energy and bandwidth. The measured spin wave excitation is significantly broader than the neutron instrument resolution, however. We attribute this to lifetime effects beyond linear spin wave theory.

The observed spin wave excitations for $Yb_2V_2O_7$ have certain similarities to those for $Yb_2Ti_2O_7$ under magnetic fields. We observe higher energy excitations in the former when compared to the latter under fields of of 5 T[14]. Correspondingly, the obtained J values for $Yb_2V_2O_7$, besides J_{zz}, are larger. (As discussed in Ref.[14], larger values of $J_{\pm}$, $J_{\pm\pm}$, and $J_{z\pm}$ produce higher energy spin wave excitations.) The large positive J_{zz} means that the strong exchange interaction in the Yb-sublattice for $Yb_2V_2O_7$ is still of the same "frustrated ferromagnetic" Ising type occurring in spin ice pyrochlores[34]. The frustration related to this easy-axis anisotropic exchange interaction in spin ice pyrochlores leads to the "two-in two-out" spin configuration on a tetrahedron[35,36] and the "three-in one-out" configuration under applied magnetic fields along the [111] axis[32,33]. Similar frustration effects in $Yb_2V_2O_7$ should also tilt the Yb^{3+} spins from the [001] towards [111] direction to form the non-collinear spin structure and stabilize the spin flop transition. In the absence of the Yb-Yb interaction our model would predict a classical Yb ordering along the [001] axis. Only with the Yb-Yb intra-lattice interaction do we find a non-collinear ground state with $\vec{M}$=($\pm$0.18,$\pm$0.18,0.97)μ_B in the global coordinate frame, in good agreement with the experimental data.

We calculated the Yb sublattice magnetization M(T) for our model within Curie-Weiss mean-field theory to determine the ordering temperature. The results (Fig. 1a) have a clear ordering temperature of $\sim$ 15 K as well as a long high-T tail extending to much higher values of T, consistent with our measurements.

VI. DISCUSSION

The non-collinear magnetic structure of Yb^{3+} observed in $Yb_2V_2O_7$ is similar to the so-called "splayed ferromagnetic state" recently observed in another Yb-pyrochlore, $Yb_2Sn_2O_7$, with non magnetic Sn^{4+} sites[37]. In $Yb_2Sn_2O_7$, the Yb^{3+} spin orders at 0.15 K with a canting angle of 10°[38] or 24°[39] from the [001] axis. In $Yb_2V_2O_7$, the Yb^{3+} spin orders at 15 K and the canting angle is 13.5°. This comparison again shows that while the V-V and Yb-V interactions increase the Yb ordering temperature by a factor of 100, the Yb-Yb interactions still maintain a non-collinear spin structure with similar canting angle. Finally, it is noteworthy that similar spin flop transitions in the [111] magnetization have been observed in $Nd_2Mo_2O_7$[40,41] and $Sm_2Mo_2O_7$[42]. In both materials, the Nd(Sm)-Mo interactions are antiferromagnetic and the ground state of Nd(Sm) ions is a "two-in two-out" ordered spin ice sate, which are different from the ferromagnetic Yb-V interactions and the non-collinear magnetic ordering of Yb ions observed here.

VII. SUMMARY

In summary, our detailed studies on $Yb_2V_2O_7$ single crystals show that V^{4+} ions ferromagnetically order at 70 K while ferromagnetic Yb-V interactions produce an ordering the Yb^{3+} spins at an increased temperature of 15 K. The Yb-Yb interactions, however, still stabilize a "splayed ferromagnetic state" and a "three-in one-out" spin flop transition with magnetic field along the [111] axis. Therefore, $Yb_2V_2O_7$ is a unique geometrically frustrated magnet exhibiting competition between intra and inter-sulabttice interactions.

Acknowledgments

The authors thank L. Balents, M. Gingras, J. Quilliam, K. Ross, and L. Savary for useful discussions and exchanges. Z.L.D. and H.D.Z. thank the support of NSF-DMR-1350002. J.G.C is supported by the National Science Foundation of China (Grant No.11304371). The work at NIST is supported in part by NSF-DMR-0944772. The work at NHMFL is supported by NSF-DMR-1157490 and the State of Florida and by the additional funding from NHMFL User Collaboration Support Grant. The work at ORNL High Flux Isotope Reactor was sponsored by the Scientific User Facilities Division, Office of Basic Energy Sciences, U.S. Department of Energy.

Appendix A: Exchange matrices

We adopt the FCC primative Bravais lattice for the pyrochlore structure with lattice constant a. The Yb atoms are located at the corners of tetrahedra whose centers lay at the FCC lattice positions. Their positions are $\mathbf{r}_0 = \frac{a}{8}[1,1,1]$, $\mathbf{r}_1 = \frac{a}{8}[1,-1,-1]$, $\mathbf{r}_2 = \frac{a}{8}[-1,1,-1]$, and $\mathbf{r}_3 = \frac{a}{8}[-1,-1,1]$. As outlined in appendix A of Ref.[14], the exchange matrices between each pair of sites can found by applying the appropriate rotations to the matrix J_{01}. The remaining matrices are

$$
\begin{aligned}
J_{02} &= \begin{pmatrix} J_1 & -J_4 & J_3 \\ J_4 & J_2 & J_4 \\ J_3 & -J_4 & J_1 \end{pmatrix} \\
J_{03} &= \begin{pmatrix} J_1 & J_3 & -J_4 \\ J_3 & J_1 & -J_4 \\ J_4 & J_4 & J_2 \end{pmatrix} \\
J_{12} &= \begin{pmatrix} J_1 & -J_3 & J_4 \\ -J_3 & J_1 & -J_4 \\ -J_4 & J_4 & J_2 \end{pmatrix} \\
J_{13} &= \begin{pmatrix} J_1 & J_4 & -J_3 \\ -J_4 & J_2 & J_4 \\ -J_3 & -J_4 & J_1 \end{pmatrix} \\
J_{23} &= \begin{pmatrix} J_2 & -J_4 & J_4 \\ J_4 & J_1 & -J_3 \\ -J_4 & -J_3 & J_1 \end{pmatrix}
\end{aligned}
$$

and $J_{ji} = J_{ij}^T$.

The exchange parameters in the local spin coordinates are:

$$
\begin{aligned}
J_{zz} &= -\frac{1}{3}(2J_1 - J_2 + 2J_3 + 4J_4), \\
J_{\pm} &= \frac{1}{6}(2J_1 - J_2 - J_3 - 2J_4), \\
J_{\pm\pm} &= \frac{1}{6}(J_1 + J_2 - 2J_3 + 2J_4), \\
J_{z\pm} &= \frac{1}{3\sqrt{2}}(J_1 + J_2 + J_3 - J_4),
\end{aligned}
$$

Appendix B: Spin wave theory

The spin-wave Hamiltonian is obtained from our effective Hamiltonian 2 in a way analogous to Ref.[14]. We introduce Holstein-Primakoff bosons $x_\alpha = x_\alpha^\dagger$ and $y_\alpha = y_\alpha^\dagger$ on each Yb site α. These operators satisfy the relations $[x_\alpha, y_\alpha] = i$ and $n_\alpha = \frac{1}{2}(x_\alpha^2 + y_\alpha^2 - 1)$ such that $\mathbf{S}_\alpha \cdot \mathbf{u}_\alpha = s - n_\alpha$, $\mathbf{S}_\alpha \cdot \mathbf{v}_\alpha = \sqrt{x}_\alpha$, and $\mathbf{S}_\alpha \cdot \mathbf{w}_\alpha = \sqrt{s} y_\alpha$. Here $\mathbf{v}_\alpha$,$\mathbf{w}_\alpha$, and $\mathbf{u}_\alpha$ are a set of orthonormal basis vectors. The vector $\mathbf{u}_\alpha$ is choosen to point in the direction of the spin $\mathbf{S}_\alpha$ of the classical ground state. The remaining vectors are constructed using $\mathbf{v}_\alpha = \mathbf{u}_\alpha \times [1,1,1]/||\mathbf{u}_\alpha \times [1,1,1]||$ and $\mathbf{w}_\alpha = \mathbf{u}_\alpha \times \mathbf{v}_\alpha$.

Since the classical ground state does not enlarge the unit cell, the Fourier transform to momentum space is straightforward. The spin wave Hamiltonian $H_\mathbf{k}$ to linear order in s has a form similar to Eq. C3 of Ref.[14] with

$$
H_\mathbf{k} = (X_{-\mathbf{k}}^T, Y_{-\mathbf{k}}^\dagger) \begin{pmatrix} A_\mathbf{k} & C_\mathbf{k} \\ C_\mathbf{k}^T & B_\mathbf{k} \end{pmatrix} \begin{pmatrix} X_\mathbf{k} \\ Y_\mathbf{k} \end{pmatrix} \tag{B1}
$$

where $(X^T Y^T) = (x_0, \ldots x_3, y_0, \ldots y_3)$. The ab elements of each matrix are defined as

$$
[D]_{ab} = [\tilde{D}]_{ab} \cos[\mathbf{k} \cdot (\mathbf{r}_a - \mathbf{r}_b)], \tag{B2}
$$

where $D = A, B, C$ and

$$
\begin{aligned}
\left[\tilde{A}\right]_{ab} &= s\left(\mathbf{v}_a^T J_{ab} \mathbf{v}_b - \mathbf{u}_a^T \sum_{c=0}^{4} J_{ac} \mathbf{u}_c + J_{V-Yb} \langle \mathbf{S}_V \rangle \cdot \mathbf{u}_a\right) \\
\left[\tilde{B}\right]_{ab} &= s\left(\mathbf{w}_a^T J_{ab} \mathbf{v}_b - \mathbf{w}_a^T \sum_{c=0}^{4} J_{ac} \mathbf{u}_c + J_{V-Yb} \langle \mathbf{S}_V \rangle \cdot \mathbf{u}_a\right) \\
\left[\tilde{C}\right]_{ab} &= s \mathbf{v}_a^T J_{ab} \mathbf{w}_b.
\end{aligned}
$$

Here, $\langle \mathbf{S}_V \rangle = \langle S_v \rangle \hat{\mathbf{z}}$ is the mean-field V spin, which points alon the z-direction in global coordinates.

[1] L. Balents, Nature **464**, 199 (2010).
[2] S. Yamashita, Y. Nakazawa, M. Oguni, Y. Oshima, H. Nojiri, Y. Shimizu, K. Miyagawa, K. Kanoda, Nature Phys. **4**, 459 (2008).
[3] S. Nakatsuji, K. Kuga, K. Kimura, R. Satake, N. Katayama, E. Nishibori, H. Sawa, R. Ishii, M. Hagiwara, F. Bridges, T. U. Ito, W. Higemoto, Y. Karaki, M. Halim, A. A. Nugroho, J. A. Rodriguez-Rivera, M. A. Green, and C. Broholm, Science **328**, 1246 (2010).
[4] J. G. Cheng, G. Li, L. Balicas, J. S. Zhou, J. B. Goodenough, C. K. Xu, and H. D. Zhou, Phys. Rev. Lett. **107**, 197204 (2011).

[5] S. S. Lee, P. A. Lee, and T. Senthil, Phys. Rev. Lett. **98**, 067006 (2007).

[6] J. S. Helton, K. Matan, M. P. Shores, E. A. Nytko, B. M. Bartlett, Y. Yoshida, Y. Takano, A. Suslov, Y. Qiu, J.-H. Chung, D. G. Nocera, and Y. S. Lee, Phys. Rev. Lett. **98**, 107204 (2007).

[7] T. H. Han, J. S. Helton, S. Y. Chu, D. G. Nocera, J. A. Rodriguez, C. Broholm and Y. S. Lee, Nature **492**, 406 (2012).

[8] Y. Ran, M. Hermele, P. A. Lee, and X. G. Wen, Phys. Rev. Lett. **98**, 117205 (2007).

[9] J. D. Thompson, P. A. McClarty, H. M. Ronnow, L. P. Regnault, A. Sorge, and M. J. P. Gingras, Phys. Rev. Lett. **106**, 187202 (2011).

[10] R. Applegate, N. R. Hayre, R. R. P. Singh, T. Lin, A .G. R. Day, and M. J. P. Gingras, Phys. Rev. Lett. **109**, 097205 (2012).

[11] K. A. Ross, L. R. Yaraskavitch, M. Laver, J. S. Gardner, J. A. Quilliam, S. Meng, J. B. Kycia, D. K. Singh, Th. Proffen, H. A. Dabkowska, and B. D. Gaulin, Phys. Rev. B **84**, 174442 (2011).

[12] K. A. Ross, J.P. C. Ruff, C. P. Adams, J. S. Gardner, H. A. Dabkowska, Y. Qiu, J. R. D. Copley, and B. D. Gaulin, Phys. Rev. Lett. **103**, 227202 (2009).

[13] L. J. Chang, S. Onoda, Y. Su, Y. J. Kao, K. D. Tsuei, Y. Yasui, K. Kakurai, and M. R. Lees, Nature Communication **3**, 992 (2012).

[14] K. A. Ross, L. Savary, B. D. Gaulin, and L. Balents, Phys. Rev. X **1**, 021002 (2011).

[15] N. R. Hayre, K. A. Ross, R. Applegate, T. Lin, R. R. P. Singh, B. D. Gaulin and M. J. P. Gingras, Phys. Rev. B **87**, 184423 (2013).

[16] R. M. D'Ortenzio, *et al.*, Phys. Rev. B **88**, 134428 (2013).

[17] J. A. Hodges, P. Bonville, A. Forget, M. Rams, K. Krolas, and G. Dhalenne, J. Phys. Condens. Matter **13**, 9301 (2001).

[18] H. Cao, A. Gukasov, I. Mirebeau, P. Bonville, C. Decorse, and G. Dhalenne, Phys. Rev. Lett. **103**, 056402 (2009).

[19] H. B. Cao, A. Gukasov, I. Mirebeau, and P. Bonville. J. Phys. Condens. Matter **21**, 492202 (2009).

[20] L. Savary and L. Balents, Phys. Rev. Lett. **108**, 037202 (2012).

[21] Y. Yasui *et al.*, J. Phys. Soc. Jpn. **72**, 3014 (2003).

[22] K. Waku, T. Suzuki, and T. Katsufuji, Phys. Rev. B **74**, 024402 (2006).

[23] S. Soderhorm and J. E. Greedan, Mater. Res. Bull **17**, 707 (1982).

[24] L. Soderholm, J. E. Greedan, M. F. Collins, J. Solid. State Chem. **35**, 385 (1980).

[25] L. Soderholm, C. V. Stager, J. E. Greedan, J. Solid. State Chem. **43**, 175 (1982).

[26] The identification of the commercial product does not indicate that it is endorsed by NIST or is recommended by NIST or that it is necessarily the best equipment for the purposes described.

[27] B. C. Chakoumakos, H. Cao, F. Ye, A. D. Stoica, M. Popovici, M. Sundaram, W. Zhou, J. S. Hicks, G. W. Lynn and R. A. Riedel, J. Appl. Cryst. **44**, 655 (2011).

[28] J. R. D. Copley and J. C. Cook, Chem. Phys. **292**, 477 (2003).

[29] J. A. Rodriguez, D. M. Adler, P. C. Brand, C. Broholm, J. C. Cook, C. Brocker, R. Hammond, Z. Huang, P. Hundertmark, J. W. Lynn, N. C. Maliszewskyj, J. Moyer, J. Orndorff, D. Pierce, T. D. Pike, G. Scharfstein, S. A. Smee and R. Vilaseca, Meas. Sci. Technol. **19** 034023 (2008).

[30] Y. Onose, T. Ideue, H. Katsura, Y. Shiomi, N. Nagaosa, Y. Tokura, Science **329**, 297 (2010).

[31] H. D. Zhou, E. S. Choi, J. A. Souza, J. Lu, Y. Xin, L. L. Lumata, B. S. Conner, L. Balicas, J. S. Brooks, J. J. Neumeier, and C. R. Wiebe, Phys. Rev. B **77**, 020411 (2008).

[32] H. Fukazawa, R. G. Melko, R. Higashinaka, Y. Maeno, and M. J. P. Gingras, Phys. Rev. B **65**, 054410 (2002).

[33] T. Sakakibara, T. Tayama, Z. Hiroi, K. Matsuhira, and S. Takagi, Phys. Rev. Lett. **90**, 207205 (2003).

[34] J. S. Gardner, M. J. P. Gingras, and J. E. Greedan, Rev. Mod. Phys. **82**, 53 (2010).

[35] A. P. Ramirez A. Hayashi, R. J. Cava, R. Siddharthan, and B.S. Shastry, Nature **399**, 333 (1999).

[36] S. T. Bramwell and M. J. P. Gingras, Science **294**, 1495 (2001).

[37] A. Yaouanc, P. Dalmas de Reotier, P. Bonville, J. A. Hodges, V. Glazkov, L. Keller, V. Sikolenko, M. Bartkowiak, A. Amato, C. Baines, P. J. C. King, P. C. M. Gubbens, and A. Forget, Phys. Rev. Lett. **110**, 127207 (2013).

[38] Z. L. Dun, E. S. Choi, H. D. Zhou, A. M. Hallas, H. J. Silverstein, Y. Qiu, J. R. D. Copley, J. S. Gardner, and C. R. Wiebe, Phys. Rev. B **87**, 134408 (2013).

[39] J. Lago, I. Zivkovic, J. O. Piatek, P. Alvarez, D. Huvonen, F. L. Pratt, M. Diaz, T. Rojo, Phys. Rev. B **89**, 024421 (2014).

[40] Y. Taguchi1, Y. Oohara, H. Yoshizawa, N. Nagaosa, Y. Tokura, Science **291**, 2573 (2001).

[41] Y. Taguchi, T. Sasaki, S. Awaji, Y. Iwasa, T. Tayama, T. Sakakibara, S. Iguchi, T. Ito, and Y. Tokura, Phys. Rev. Lett. **90**, 257202 (2003).

[42] S. Singh, R. Suryanarayanan, R. Tackett, G. Lawes, A. K. Sood, P. Berthet, and A. Revcolevschi, Phys. Rev. B **77**, 020406 (2008).

[43] The coupling between the Yb and V sublattices can of course be anisotropic. Our assumption of an isotropic coupling can be viewed as a minimal model.